Superior output linearity of optimized double heterostructure vertical-cavity top-emitting lasers

L. W. Tu,[a] E. F. Schubert, Y. H. Wang, B. E. Weir, G. J. Zydzik, and A. Y. Cho
AT&T Bell Laboratories, Murray Hill, New Jersey 07974

(Received 18 May 1994; accepted for publication 17 February 1995)

Optimized double heterostructure (DH) vertical-cavity top-emitting lasers are grown by molecular beam epitaxy. Both the doping profile and the laser structure are optimized to achieve high performance. Continuous wave 2 mW output power at room temperature is obtained for nominal 10 μm diam DH vertical-cavity top-emitting injection lasers. A single fundamental longitudinal and transverse mode is maintained up to 1.7 mW. It lases in continuous waves at a temperature of 80 °C. A lasing power range of ~0.8 mW is sustained within a 10% change in the output linearity, which is much larger than a value of less than 0.1 mW for quantum well lasers. This demonstrates that its output linearity is far more superior than the one of compared quantum well lasers, which is explained in detail. © *1995 American Institute of Physics.*

Various structures and properties of vertical-cavity surface-emitting lasers (VCSELs) have been studied intensively in recent years.[1–9] Advantages known in VCSELs are their microscopic sizes, low threshold currents, circular beams, planar structures, and surface emitting geometry. On the other hand, attempts are underway to improve their output power, heat reduction/dissipation, and beam polarity, and to engineer simpler structures, and simplified processing. Particularly, output linearity is important in various potential applications. Premature saturation and nonlinear behavior of the output power are major areas under intensive investigation in VCSELs.

Double heterostructure (DH) structure is advantageous in terms of simpler design, fewer interfaces in the active region, better control in the growth, and higher yield, as compared with quantum well (QW) structures. In this work, laser structure is optimized by (i) designing the position of the active region to be coincident with the position of maximum electric field intensity to increase the gain per unit length by a factor of 2 as compared with a uniform medium,[10] (ii) having linearly graded confinement layers cladded on both sides of the active region to effectively confine the charge carriers,[11] and (iii) shaping the doping profile according to the resonant field intensity to minimize the free-carrier absorption while maximizing the conductivity to reduce heat generation. Direct current injection is used for all the experiments at room temperature or above.

The whole DH GaAs/AlGaAs laser structures are grown in a Riber 2300 molecular beam epitaxy system. The active region is 720 Å thick, undoped GaAs. The 2250 Å thick confinement layers are graded $Al_xGa_{1-x}As$ with x linearly varied from 0.3 to 0.6, undoped near the active region, Si doped to 1×10^{18} cm^{-3} adjacent to the bottom mirror, and Be doped to 3×10^{18} cm^{-3} adjacent to the top mirror. The top p-type mirror is a 20-period, two-step graded distributed Bragg reflector (DBR) with a structure of $Al_{0.14}Ga_{0.86}As$ (430 Å)/$Al_{0.4}Ga_{0.6}As$ (100 Å)/$Al_{0.7}Ga_{0.3}As$ (100 Å)/AlAs (520 Å).[12] The first five periods near the active region are Be doped to 3×10^{18} cm^{-3}, and then the doping concentration is raised to 6×10^{18} cm^{-3}, and ended with $\sim1\times10^{19}$ cm^{-3} at the surface for ohmic contact formation. The bottom n-type mirror is a 30-period, two-step graded DBR, and Si doped to 1×10^{18} cm^{-3}. The substrates are n-type, heavily Si-doped (001)GaAs.

Shown in Fig. 1(a) is the resonant field pattern inside the laser cavity. It is calculated from the superposition of two traveling waves, traveling in the opposite direction along the cavity. The optical field is well confined around the gain region, and diminishes fast inside the mirror structures. The real part of the refractive index is shown in Fig. 1(b). Extremely high reflectivity quarter-wavelength DBRs are on the top and the bottom of the laser structure. Note that the position of the GaAs active region is in an antinode position, where the optical field intensity is a maximum. This optimized position alignment results in lower threshold current,

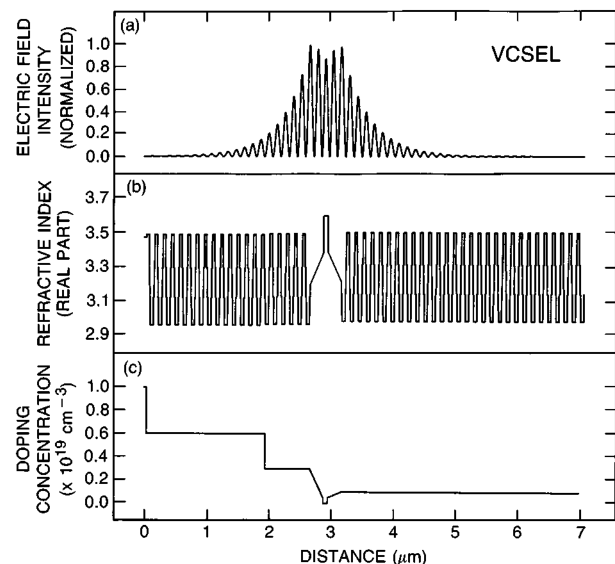

FIG. 1. (a) Resonant field distribution inside the laser cavity. (b) Real part of the refractive index of the laser structure. (c) Optimized doping profile of the lasers.

[a]Electronic mail: lwt@mhcnet.att.com

 0003-6951/95/66(18)/2315/3/$6.00 © 1995 American Institute of Physics

Downloaded¬27¬Jun¬2003¬to¬128.113.111.105.¬Redistribution¬subject¬to¬AIP¬license¬or¬copyright,¬see¬http://ojps.aip.org/aplo/aplcr.jsp

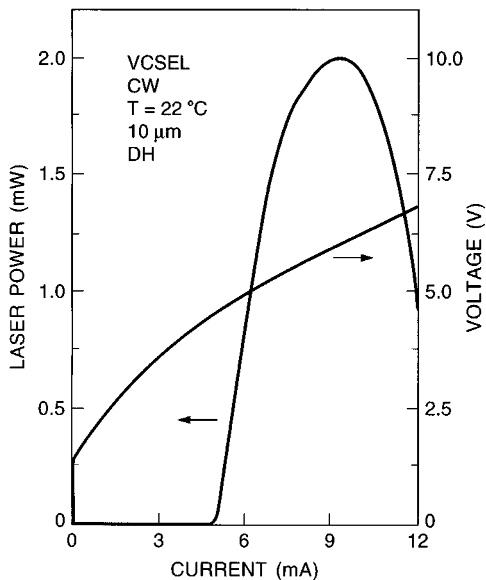

FIG. 2. Continuous wave light output power and voltage characteristic vs injection current at room temperature. Single fundamental mode with 1.7 mW is obtained for nominal 10 μm devices.

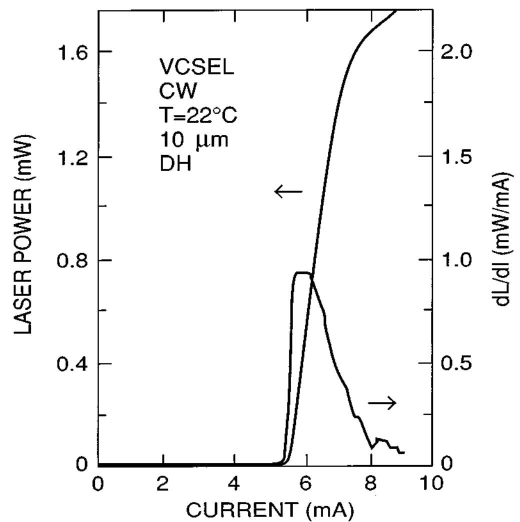

FIG. 3. Light output linearity shown as dL/dI vs excitation current for DH structure which shows a much superior output linearity than the QW structure shown in Fig. 4.

and higher output power. Figure 1(c) is the doping profile of the laser structure which is described in detail in the previous paragraph. Since the series resistance of the device is largely due to the top p-type DBR mirror, the doping profile is particularly engineered to lower the series resistance by higher doping in the p-type DBR than the n-type DBR. In the mean time, the doping profile is tailored to lower the free-carrier absorption by lighter doping in high optical field intensity region as shown in Fig. 1(c).

To fabricate the devices, 300 keV protons are implanted in a dose of 5×10^{14} cm^{-2}. The calculated mean stop range is ~2.6 μm. Its position is just above the active region to shape the current flow path. Devices of interest are protected with a 6.2 μm thick, 10 μm in diameter photoresist. Ohmic contact with ~1500 Å thick Au/Be on the top of the p-type mirror is achieved by electron beam evaporation. The opening window for light output is revealed after the lift off of the thick photoresist. The next step is mesa etching using a solution of H_2SO_4:H_2O_2:H_2O=1:1:6 to a depth of ~2.8 μm. The substrate is bonded with a conductive epoxy on a copper slab which serves as a heat sink. Under the heat sink, there is a thermoelectric heat-pump module used to increase the temperature of the heat sink. A thermometer is bonded to the copper slab with a heat sink compound to monitor the temperature of the heat sink. Direct current is injected into the laser cavity through the Au/Be contact pad using a very fine probe. The light output power versus current $(L-I)$ and voltage versus current characteristics $(V-I)$ are measured with an HP-4145B semiconductor parameter analyzer and a calibrated Si photodiode. The near field pattern is analyzed through a vidicon and a video analyzer.

The cw light output power and the diode voltage versus injection current at room temperature are shown in Fig. 2. This device lases at a wavelength of 0.89 μm with a threshold current of 4.6 mA. The voltage at lasing threshold is 4.5 V for this device. The output power increases linearly from the threshold to about 1.7 mW at a current of ~7.8 mA, where a slight kink is observable. In the measurement of the lasing spectra with a resolution better than 0.1 Å, a single lasing peak is observed as the excitation current raised above the threshold. As the excitation current increases to ~7 mA, another lasing peak starts to show up. This higher transverse mode peak appears at a position of 6 Å shorter in the wavelength from the fundamental transverse mode peak. At ~9 mA, the laser output power reaches 2 mW.

To study the linearity of the output power, a dL/dI curve is plotted against the injected current as in Fig. 3. It is compared with Fig. 4 for a QW sample which has a three-QW, GaAs/AlGaAs(100 Å/80 Å) design and is grown from the same system under similar conditions in a successive run. It lases at 0.88 μm with a threshold of 4 mA and a power in the vicinity of 1.5 mW. The threshold currents are in the range of 2.2–4.2 mA for QW samples as compared with

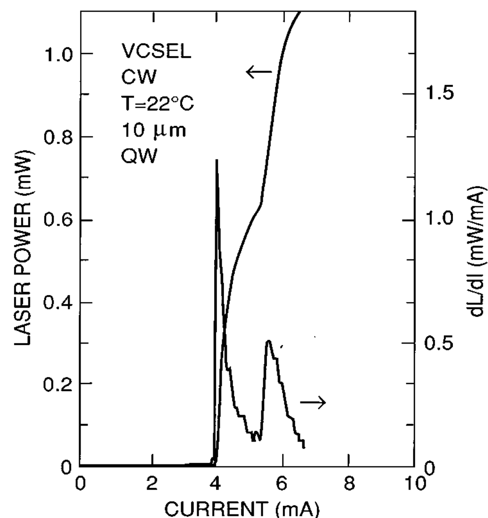

FIG. 4. Light output linearity shown as dL/dI vs excitation current for QW structure as compared with DH structure shown in Fig. 3.

Downloaded¬27¬Jun¬2003¬to¬128.113.111.105.¬Redistribution¬subject¬to¬AIP¬license¬or¬copyright,¬see¬http://ojps.aip.org/aplo/aplcr.jsp

DH samples 2.9–5.5 mA. Within a 10% change in the dL/dI curve centered around the curve maximum, DH structure sustains a lasing power range of ~0.8 mW, while in the contrast of the QW structure, it is less than 0.1 mW. The DH structure shows a much more superior linearity in the output power than the QW structure, and this is ascribed to the different characteristics of the gain spectra.[13,14] Both DH and QW lasers lase at a wavelength longer than their gain peak wavelengths determined from the spontaneous emission measurements. It is estimated to be about 50 Å longer in wavelength at threshold. As the excitation current increases, the gain peak redshifts in a speed of ~3 Å/°C around room temperature. It can be estimated with[15] $E_g(T)=1.519-5.405\times10^{-4}\ T^2/(204+T)$, where E_g is in eV and T in K. This redshift of the gain peak is relatively faster than the redshift of the Fabry–Pérot (FP) mode (~1 Å/°C) as the cavity temperature increases. For a DH structure, the gain spectrum is a rather smooth-varying curve due to its parabolic density of states. While for a QWstructure, the gain spectrum has a multiple-peak structure due to its quantized transitions and steplike density of states.[16] Lasing occurs near the maximum gain peak which is a relatively sharp structure due to the quantum size effect which widens the energy gap between the transition subbands, and increases the density of states as the well width decreases. Therefore, the variation of the gain value as the FP mode sweeping across the gain spectrum is larger and faster as compared with DH structure. These differences reflect on the sharper change in the dL/dI curve for the QW structure. Another possible factor is that the DH structure has a larger nonradiative recombination time and a lower internal loss due to less heterostructure interfaces in the critical active region than a QW structure.[17] Both DH and QW lasers lase at a longer wavelength than expected mainly due to the excess joule heat. And the early onset of the kink in Fig. 4 is also ascribed to the excess heat near the thin active layer.

Near field pattern shows a nearly perfect circular geometry which enables ultrahigh coupling efficiency with optical fiber. Intensity profile is measured, and a Gaussian distribution with a full width at half-maximum (FWHM) of 7 μm is obtained. At the excitation current where the slight kink shows up in the $L-I$ curve, the near field pattern starts to deviate from the circular pattern. Higher mode patterns appear as the excitation current increases to higher values. As combined with the light output power and the lasing spectrum measurements, it concludes that the lasing is in the single fundamental transverse mode up to 1.7 mW.

This work demonstrates the high performance VCSELs using a simpler DH structure. Continuous wave 2 mW output power at room temperature for nominal 10 μm devices is achieved. A single fundamental transverse mode is in operation up to 1.7 mW with a circular near field beam pattern, and a Gaussian distribution. Continuous wave lasing is maintained at a temperature of 80 °C. The output power linearity is much superior than compared QW structure, which is a manifestation of the difference in the gain spectra, and the advantageous aspect of a DH structure. Even higher output power is expected with further reduced series resistance.

[1] K. Iga, F. Koyama, and S. Kinoshita, IEEE J. Quantum Electron. **QE-24**, 1845 (1988).
[2] E. F. Schubert, L. W. Tu, R. F. Kopf, G. J. Zydzik, and D. G. Deppe, Appl. Phys. Lett. **57**, 117 (1990).
[3] L. W. Tu, E. F. Schubert, R. F. Kopf, G. J. Zydzik, M. Hong, S. N. Chu, and J. P. Mannaerts, Appl. Phys. Lett. **57**, 2045 (1990).
[4] C. J. Chang-Hasnain, M. W. Maeda, N. G. Stoffel, J. P. Harbison, and L. T. Florez, Electron. Lett. **26**, 940 (1990).
[5] J. L. Jewell, J. P. Harbison, A. Scherer, Y. H. Lee, and L. T. Florez, IEEE J. Quantum Electron. **QE-27**, 1332 (1991).
[6] L. W. Tu, E. F. Schubert, H. M. O'Bryan, Y. H. Wang, B. E. Weir, G. J. Zydzik, and A. Y. Cho, Appl. Phys. Lett. **58**, 790 (1991).
[7] L. W. Tu, Y. H. Wang, E. F. Schubert, B. E. Weir, G. J. Zydzik, and A. Y. Cho, Electron. Lett. **27**, 457 (1991).
[8] R. S. Geel, B. J. Thibeault, S. W. Corzine, J. W. Scott, and L. A. Coldren, IEEE J. Quantum Electron. **QE-29**, 2977 (1993).
[9] E. F. Schubert, L. W. Tu, G. J. Zydzik, R. F. Kopf, A. Benvenuti, and M. R. Pinto, Appl. Phys. Lett. **60**, 466 (1992).
[10] M. Y. A. Raja, S. R. J. Brueck, M. Osinski, C. F. Schaus, J. G. McInerney, T. M. Brennan, and B. E. Hammons, Electron. Lett. **24**, 1140 (1988).
[11] W. T. Tsang, Appl. Phys. Lett. **39**, 134 (1981).
[12] K. Tai, L. Yang, J. D. Wynn, and A. Y. Cho, Appl. Phys. Lett. **56**, 2496 (1990).
[13] Y. Arakawa and A. Yariv, IEEE J. Quantum Electron. **QE-22**, 1887 (1986).
[14] B. Saint-Cricq, F. Lozes-Dupuy, and G. Vassilieff, IEEE J. Quantum Electron. **QE-22**, 625 (1986).
[15] C. D. Thurmond, J. Electrochem. Soc. **122**, 1133 (1975).
[16] Y. Arakawa and A. Yariv, IEEE J. Quantum Electron. **QE-21**, 1666 (1985).
[17] G. P. Agrawal and N. K. Dutta, *Semiconductor Lasers*, 2nd ed. (Van Nostrand Reinhold, New York, 1993), Chaps. 2 and 3.

Downloaded¬27¬Jun¬2003¬to¬128.113.111.105.¬Redistribution¬subject¬to¬AIP¬license¬or¬copyright,¬see¬http://ojps.aip.org/aplo/aplcr.jsp